Mon. Not. R. Astron. Soc. **391,** 685–699 (2008) doi:10.1111/j.1365-2966.2008.13866.x

# Galaxy populations in the Antlia cluster – II. Compact elliptical galaxy candidates⋆

Analía V. Smith Castelli,[1,2,3]† Favio R. Faifer,[1,2,3]† Tom Richtler[4]† and Lilia P. Bassino[1,2,3]†

[1] *Facultad de Ciencias Astronómicas y Geofísicas, Universidad Nacional de La Plata, Paseo del Bosque, B1900FWA La Plata, Argentina*
[2] *Instituto de Astrofísica de La Plata (CCT La Plata - CONICET - UNLP), Paseo del Bosque, B1900 FWA La Plata, Argentina*
[3] *Consejo Nacional de Investigaciones Científicas y Técnicas, Rivadavia 1917, Buenos Aires, Argentina*
[4] *Departamento de Astronomía, Universidad de Concepción, Casilla 160-C, Concepción, Chile*

Accepted 2008 August 19. Received 2008 August 19; in original form 2008 June 21



**ABSTRACT**

Continuing our study of galaxy populations in the Antlia cluster, we present a photometric analysis of four galaxies classified as compact elliptical (cE) galaxies in the 1990 Antlia Group catalogue of Ferguson and Sandage. Until now, there have been only six known members of this rare type of galaxy. Using data from various photometric systems (Washington *C*, Kron–Cousins *R*, Bessel *V* and *I*, *Hubble Space Telesecope F*814*W* and *F*435*W*), we measured the brightness and colour profiles, as well as the structural parameters. By comparing these with those of other galaxies in the Antlia cluster, as well as with confirmed cE galaxies from the literature, we found that two of the cE candidates, although spectroscopically confirmed Antlia members, are not cE galaxies. However, one of these objects presents strong ellipticity and position angle variations that resemble those already reported for M32, leading us to speculate about this type of object being a progenitor of a cE galaxy. The other two cE candidates, for which radial velocities are not available, match some features typical of cE galaxies, such as being close in projection to a larger galaxy, displaying flat colour profiles, and having a high degree of compactness. Only one of the remaining cE candidates shows a high central surface brightness, two components in its brightness profile and distinct changes in ellipticity and position angle where the outer component begins to dominate. It seems to follow the same trend as other confirmed cE galaxies in a luminosity versus mean effective surface brightness diagram. Moreover, it shows a distorted inner structure with similar characteristics to those found by simulations of interacting galaxies. Also, an extremely faint structure, which seems to link this object with one of the Antlia dominant galaxies, has been detected in images from the Cerro Tololo Inter-American Observatory MOSAIC, the Very Large Telescope FORS1 and the *Hubble Space Telescope* Advanced Camera for Surveys. The cE nature of this galaxy and the possible interaction with its bright companion still have to be confirmed using spectroscopy.

**Key words:** galaxies: clusters: general – galaxies: clusters: individual: Antlia – galaxies: dwarf – galaxies: elliptical and lenticular, cD – galaxies: peculiar – galaxies: photometry.

## 1 INTRODUCTION

Early-type dwarf galaxies are the most frequent galaxy type in nearby groups and clusters of galaxies (e.g. Ferguson & Sandage 1990, hereafter FS90). Although the information related to their evolution in such environments is codified in their spatial distribution, chemical composition and kinematics, a single scenario including all their properties in a consistent frame is still missing. The main difficulty lies in the fact that they do not constitute a homogeneous class of objects. Among them, there are nucleated and non-nucleated galaxies, as well as systems that have been found to

⋆This paper is based on observations carried out at the Cerro Tololo Inter-American Observatory (Chile), at Las Campanas Observatory (Chile), and at the European Southern Observatory, Paranal (Chile) [Program 71.B-0122(A)]. It is also based on observations made with the NASA/ESA *Hubble Space Telescope*, obtained from the data archive at the Space Telescope Science Institute, which is operated by the association of Universities for Research in Astronomy, Inc., under NASA contract NAS 5-26555.

†E-mail: asmith@fcaglp.unlp.edu.ar (ASC); favio@fcaglp.unlp.edu.ar (FF); tom@mobydick.cfm.udec.cl (TR); lbassino@fcaglp.unlp.edu.ar (LB)

harbour discs and spiral structure (Jerjen, Kalnajs & Binggeli 2000; Graham, Jerjen & Guzmán 2003; Cellone & Buzzoni 2005; Lisker, Grebel & Binggeli 2006b). Moreover, central star formation has also been reported in some objects (Lisker et al. 2006a).

The so-called compact elliptical (cE; e.g. Nieto & Prugniel 1987), compact dwarf elliptical (cdE; Drinkwater et al. 2001) or M32-like (e.g. Ziegler & Bender 1998) galaxies are members of the low-luminosity galaxy family. However, instead of having low surface brightness, as the most common early-type dwarfs do, they have notorious high surface brightness (e.g. Nieto & Prugniel 1987). They constitute a very rare group, as there are many galaxies classified as cEs (see, for instance, Binggeli, Sandage & Tammann 1985), but only five objects have been confirmed as such, in addition to the prototype M32 (see Graham 2002 for an alternative interpretation).

The known examples are all companions of larger galaxies. They are M32 itself, a satellite of the M31 (Andromeda) spiral galaxy, NGC 4486B close to M87 in the Virgo cluster (Sandage & Binggeli 1984; Davidge 1991), NGC 5846A close to the giant elliptical NGC 5846 (Davidge 1991; Mahdavi, Trentham & Tully 2005), A496cE close to the cluster dominant (cD) galaxy of the cluster Abell 496 (Chilingarian et al. 2007), and two objects in the Abell 1689 cluster ($CG_{A1689,1}$ and $CG_{A1689,2}$; Mieske et al. 2005). It should be noted that object $CG_{A1689,1}$ from Mieske et al. (2005) has a deviating radial velocity with respect to its closest projected giant elliptical.

In particular, M32 presents the following characteristics:

(i) it is a satellite of a larger galaxy;

(ii) the brightness profile cannot be accurately fitted with a single Sérsic law (Choi, Guhathakurta & Johnston 2002; Graham 2002);

(iii) it has high surface brightness in comparison with ellipticals of the same luminosity (Nieto & Prugniel 1987) and correspondingly a small size (Choi et al. 2002; Graham 2002);

(iv) it has a radial change in both age and metallicity, leading to a flat colour profile, its stellar population being younger and more metal-rich at the centre (Rose et al. 2005).

The other confirmed cE galaxies show similar properties with respect to surface brightness, compactness and projected location close to brighter galaxies. However, there might be some differences in their colour gradients and brightness profiles (see, for example, Lauer et al. 1996; Ferrarese et al. 2006, regarding NGC 4486B) as well as in metal content and age (e.g. Sánchez-Blázquez, Gorgas & Cardiel 2006; Chilingarian et al. 2007).

Some effort has been made to find more examples of these very rare objects in nearby clusters or groups, such as Fornax (Drinkwater et al. 2001) and Leo (Ziegler & Bender 1998). However, all the examined candidates have been rejected as cE galaxies. As the questions related to their origin and their role in the framework of galaxy evolution remain open still, it would be of great interest to find more objects and to study them in relation to their environment.

The Antlia cluster of galaxies is the third nearest well-populated galaxy cluster after Virgo and Fornax. It exhibits a complex structure consisting of several subgroups, the most conspicuous being dominated by the giant elliptical galaxies NGC 3258 and NGC 3268. X-ray observations showed extended emissions around both subgroups (Pedersen, Yoshii & Sommer-Larsen 1997; Nakazawa et al. 2000). These emissions are concentrated towards the dominant galaxies, but extensions elongated in the direction to the other subgroup are also present, suggesting an ongoing merger. Dirsch, Richtler & Bassino (2003) and Bassino, Richtler & Dirsch (2008) have shown that the globular cluster systems around NGC 3258 and NGC 3268 are elongated in the same direction as a connecting line between the two galaxies, resembling the X-ray results.

The photographic survey of FS90 was the first and last major effort devoted to studying the galaxy population of the Antlia cluster. They identified, by visual inspection, 375 galaxies that are listed in their Antlia Group Catalogue (hereafter labelled by the acronym FS90 plus the catalogue number). It gives, among other data, a membership status (1, definite member; 2, likely member; 3, possible member) and a morphological type for each galaxy. FS90 classified 10 objects as E(M32?) or S0(M32?) and one object as d:E(M32?),N.

Given the lack of an extensive analysis of Antlia's galaxy population, we initiated the Antlia Cluster Project with the aim of performing the first CCD photometric and spectroscopic study of this cluster. In the first paper of this long-term project (Smith Castelli et al. 2008, hereafter Paper I), we presented photometric properties of the early-type galaxy population. Among our results, it was found that early-type members define a tight colour–magnitude relation, spanning 9 mag from giant ellipticals to dwarf galaxies, without a perceptible change of slope. This slope is similar to those found in other clusters such as Virgo, Fornax, Perseus and Coma, which are dynamically different from Antlia. It is also consistent with that displayed by the so-called 'blue tilt' of metal-poor globular clusters in NGC 4486 (Forte, Faifer & Geisler 2007).

Within the sample in Paper I, there were four galaxies classified as cE candidates by FS90. Two of these objects are spectroscopically confirmed Antlia members that seem to be normal low-luminosity early-type galaxies. The other two are each close in projection to either one of the dominant galaxies, and are separated from the locus of the early-type members in the luminosity–mean effective surface brightness diagram. They display some characteristics of cE galaxies, but radial velocities are not available.

In this paper, the second of the Antlia Cluster Project, we present a photometric analysis of four FS90 cE candidates (i.e. FS90 110, FS90 165, FS90 192 and FS90 208) located in the central region of the Antlia cluster. We aim to obtain photometric evidence in favour of, or against, these objects being genuine cE galaxies. Given the small number of cE galaxies known to date, any additional members of this class could give important clues about their evolutionary path. The central question is probably whether they have been dynamically transformed by interaction with a massive galaxy.

Throughout this paper, we adopt $(m - M) = 32.73$ as the Antlia distance modulus (Dirsch et al. 2003), which corresponds to an Antlia distance of 35.2 Mpc. At this distance, 1 arcsec subtends 170 pc. The paper is organized as follows. In Section 2 we give information about our photometric data. In Sections 3 and 4 we present an analysis of the data, and in Section 5 we give a discussion and our conclusions.

## 2 DATA

### 2.1 Observations

The data set comprises Kron–Cousins *R* and Washington *C* (Canterna 1976) images obtained with the MOSAIC camera (eight CCD mosaic imager) mounted at the prime focus of the 4-m Blanco telescope at the Cerro Tololo Inter-American Observatory (CTIO), during 2002 April 4–5. These images cover the central part of the Antlia cluster (Fig. 1) and were used for Paper I. One pixel of MOSAIC subtends 0.27 arcsec on the sky, which results in a field of view of $36 \times 36$ arcmin$^2$ (i.e. about $370 \times 370$ kpc$^2$ at the Antlia

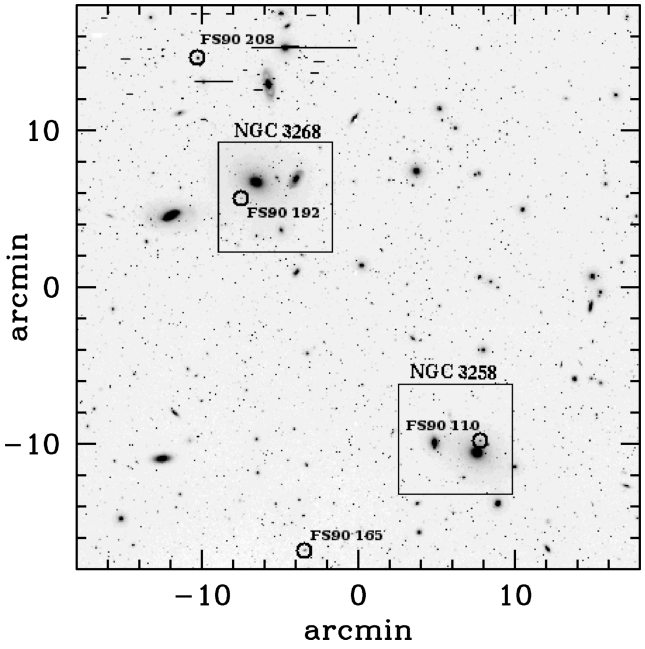


**Figure 1.** *R* image of the MOSAIC field. We show the positions of the two FORS1 fields centred on NGC 3258 and NGC 3268, respectively. The open circles indicate the locations of the FS90 cE candidates in the central region of Antlia. At the adopted Antlia distance, 1 arcmin = 10.2 kpc. North is up and east is to the left.

distance). The seeing on the *R* image is 1 arcsec and on the *C* image 1.1 arcsec. We refer to Dirsch et al. (2003) for more details.

We selected the Kron–Cousins *R* filter instead of the original Washington $T_1$ because of its better transmission at all wavelengths (Geisler 1996). *R* and $T_1$ magnitudes are very similar, with just a very small colour term and zero-point difference ($R - T_1 \approx -0.02$). We have transformed *R* magnitudes into $T_1$ magnitudes by the calibration given in Dirsch et al. (2003).

As a supplement to the MOSAIC observations, we use Bessel *V* and *I* images for two fields centred on NGC 3258 and NGC 3268, respectively, which were obtained during 2003 March 27–28 with FORS1 at the 8-m Very Large Telescope (VLT) UT1 (Antu; Cerro Paranal, Chile). These images cover two FS90 cE candidates (FS90 110 and FS90 192), are deeper and have higher resolution than those from CTIO. One pixel of this camera subtends 0.2 arcsec on the sky, giving a field of view of 6.8 × 6.8 arcmin$^2$ (i.e. 60 × 60 kpc$^2$ at the Antlia distance). The seeing on the *V* image is 0.53 arcsec for the NGC 3258 field, and 0.54 arcsec for the NGC 3268 field. We refer to Bassino et al. (2008) for more details.

In addition, we have combined four F814W band images of 570 s each, and four F435W band frames of 1340 s each, obtained from the *Hubble Space Telescope* (*HST*) Advanced Camera for Surveys (ACS) archive and centred on NGC 3258, as well as four images in the same bands and with the same exposure times, centred on NGC 3268 (proposal ID, 9427; PI, W. Harris). The FS90 cE candidates covered by these frames are, once more, FS90 110 and FS90 192. In order to make a comparison between these two candidates with a confirmed cE galaxy, we have also combined two images in the F850LP band, of 560 s each, of NGC 4486B, obtained from the same archive (proposal ID, 9401; PI, P. Côté).

All ACS images were processed with the standard calibration pipeline (CALACS + multidrizzle), including bias, dark and flat-fielding corrections. The *HST* images have a FWHM of 0.1–0.12 arcsec, one pixel of the ACS camera subtends 0.05 arcsec on the sky, and its field of view is 202 × 202 arcsec$^2$ (i.e. 34.3 × 34.3 kpc$^2$ at the Antlia distance). Following Sirianni et al. (2005), the F850LP was calibrated to the *z* band. Additionally, and adopting the transformation for $(B–I) > 1$, the F814W filter was calibrated in Cousins *I*-band magnitudes, and the F435W filter in Johnson *B*-band magnitudes.

### 2.2 Photometry

We calculated total $T_1$ magnitudes and $(C–T_1)$ colours by numerically integrating the observed brightness profiles of our FS90 cE candidates. To obtain these profiles, we applied the task ELLIPSE within IRAF (Jedrzejewski 1987). For each galaxy, we used the *R* MOSAIC image to obtain the elliptical apertures to be used also for the *C* image. These apertures were determined allowing their centres, ellipticities and position angles to vary freely, until their fits became unstable as a consequence of the low surface brightness. At this point, the three parameters were fixed in order to extend the isophotal fit as much as possible towards larger radii. The sky level was determined following the procedure described in Paper I.

The central regions of FS90 110, FS90 165 and FS90 208 were overexposed on the long-exposure images. To include these, we worked with both long- and short-exposure frames following the procedure described in Paper I for bright galaxies with overexposed centres (see also Section 3.2).

FS90 110 and FS90 192 are projected close to NGC 3258 and NGC 3268, respectively. As a consequence, they are embedded within the light of their bright companions. To obtain their brightness profiles, we constructed two-dimensional models of both dominant galaxies, and subtracted these from the original images. To build these models, we used the task BMODEL within IRAF, which creates a two-dimensional image file containing a noiseless photometric model of a source image. The models are based on the isophotal analyses previously performed with ELLIPSE. We chose a spline function for the interpolation, which is supposed to give the smallest residuals.

In order to ensure the best quality of our models, we performed two sequences of modelling and subtraction. The first models of NGC 3258/3268, built after masking out the neighbouring bright galaxies, served to enable the modelling of the companion galaxies. These models are then subtracted from the original images, after which we obtain the final models of the dominant galaxies. The subtraction of these last models for NGC 3258 and NGC 3268 from the original images provides the frames in which the profiles of FS90 110 and FS90 192 are measured, following the fitting procedure mentioned above.

The FORS *V* images were used to determine the isophotal apertures to be measured also on the FORS *I* frames, and single sequences of modelling and subtraction of the dominant galaxies were applied. The fitting procedure was similar to that performed on the MOSAIC images. This is also valid for the ACS images.

Table 1 lists relevant information about our cE candidates. In the first five columns, we show the FS90 number, positions, FS90 morphology and $E(B - V)$ values. The next six columns give the photometric results obtained in the Washington photometric system. These are the observed total magnitudes and colours (not corrected by absorption or reddening) with uncertainties in parentheses (obtained as described in Paper I), the surface brightness of the limiting isophote within which the total magnitude has been calculated, the equivalent radius of the limiting isophote, the mean surface brightness within the effective radius, and the effective radius (i.e. the

**Table 1.** FS90 cE candidates located in our MOSAIC field of the Antlia cluster. Coordinates have been obtained through CDS, which are calculated from FS90. Extinction values are from Schlegel, Finkbeiner & Davis (1998). $\mu_{T_1}$ corresponds to the surface brightness of the outermost isophote within which integrated magnitudes and colours were measured. $r_{T_1}$ is the equivalent radius ($r = \sqrt{ab} = a\sqrt{1-\epsilon}$) of that isophote. $\langle\mu_{\rm eff}\rangle$ is obtained within $r_{\rm eff}$, the radius that contains half of the light. All these values were obtained from ELLIPSE. The radial velocities are from 6dF.

| FS90 ID | RA (J2000) | Dec. (J2000) | FS90 morph. | $E(B-V)$ (mag) | $T_1$ (mag) | $(C-T_1)$ (mag) | $\mu_{T_1}$ (mag arcsec$^{-2}$) | $r_{T_1}$ (arcsec) | $\langle\mu_{\rm eff}\rangle_{T_1}$ (mag arcsec$^{-2}$) | $r_{{\rm eff}_{T_1}}$ (arcsec) | $v_{\rm r}$ (km s$^{-1}$) |
|---|---|---|---|---|---|---|---|---|---|---|---|
| 110 | 10:28:53.0 | −35:35:24 | E(M32?) | 0.085 | 15.49 (0.01) | 2.06 (0.02) | 27.5 | 14.0 | 18.4 | 1.5 | – |
| 165 | 10:29:46.0 | −35:42:25 | S0(M32?) | 0.086 | 15.50 (0.01) | 2.01 (0.02) | 27.3 | 20.9 | 20.3 | 3.6 | $2605 \pm 80$ |
| 192 | 10:30:04.5 | −35:20:31 | E(M32?) | 0.104 | 16.66 (0.01) | 2.11 (0.02) | 27.6 | 11.4 | 19.8 | 1.7 | – |
| 208 | 10:30:18.7 | −35:11:49 | S0(M32?) | 0.103 | 14.76 (0.01) | 1.94 (0.03) | 27.5 | 30.1 | 19.8 | 4.1 | $1774 \pm 100$ |

radius containing half of the light). The last column gives the heliocentric radial velocities, when available.

## 3 ANALYSIS OF MOSAIC DATA

### 3.1 Morphology and spatial location

The left column of Fig. 2 shows the morphologies of the FS90 cE candidates in the MOSAIC *R* frames. Each side is 1 arcmin (10.2 kpc at the adopted Antlia distance). In the case of FS90 110, a model of NGC 3258 has been subtracted.

FS90 110 is located at a radial distance of 47 arcsec (∼8 kpc at the Antlia distance) from NGC 3258 to the north. There is no radial velocity available for this object. FS90 110 was catalogued by FS90 as a 'possible' (i.e. status 3) Antlia member with an E(M32?) morphology. It resembles a cE galaxy (see Fig. 2), as it is round and small in projected size ($r_{T_1} \sim 2.4$kpc). It is the closest galaxy in projection to either one of the dominant Antlia galaxies and, interestingly, its *R* image shows an elongation of the outer isophotes towards its bright companion (see Fig. 2). This low surface brightness feature is seen on the *C* image as well.

FS90 165 is located at 12.2 arcmin (∼124.4 kpc at the Antlia distance) from NGC 3258 towards the south-east, and is a spectroscopically confirmed Antlia member. It was catalogued by FS90 as a 'likely' (i.e. status 2) member of Antlia with an S0(M32?) morphology. FS90 165 is one of the smallest S0 galaxies in the central region of Antlia. It is fainter than $T_1 = 14$ mag, the limiting magnitude that separates dwarfs from bright early-type galaxies in our Paper I sample.

FS90 192 is located at 1.4 arcmin (∼14.2 kpc at the Antlia distance) from NGC 3268 to the south-east. No radial velocity is available. It is catalogued as a 'possible' (i.e. status 3) Antlia member displaying an E(M32?) morphology. It looks round and compact like FS90 110, albeit smaller ($r_{T_1} \sim 1.9$ kpc at the Antlia distance; see Table 1). It is more distant in projection from NGC 3268 than FS90 110 is from NGC 3258, and there is no visible distortion in its outer isophotes.

FS90 208 is a confirmed Antlia member located at 8.5 arcmin (∼86.7 kpc at the adopted Antlia distance) from NGC 3268 to the north-east. It is considered to be a S0(M32?) 'definite' (i.e. status 1) member of Antlia by FS90. It displays a round morphology in its central region and is elongated outwards. It is the largest FS90 cE candidate in the central region of Antlia (see Table 1).

### 3.2 Brightness and colour profiles

As mentioned above, the left column of Fig. 2 shows contour plots superimposed on the *R* images of the FS90 cE candidates. We also present their $(C-T_1)$ colour profiles and the ELLIPSE B4 index versus equivalent radius (middle column), as well as the ellipticity ($\epsilon$) and position angle ($\theta$) versus equivalent radius (right column). Positive angles are measured from north to east.

Fig. 3 shows the brightness profiles for these four galaxies. From these plots, it can be seen that, if we exclude the region affected by seeing ($r < 1$ arcsec), FS90 165 and FS90 192 show what seems to be a one-component profile with smooth variations in ellipticity and position angle. In contrast, the brightness profiles of FS90 110 and FS90 208 seem to present two components in agreement with the strong changes both in ellipticity and orientation displayed by the fitted apertures.

To test whether single-component models provide good fits to the brightness profiles of the FS90 cE candidates, we used the Sérsic law (Sérsic 1968):

$$\mu(r) = \mu_0 + 1.0857 \left(\frac{r}{r_0}\right)^N. \quad (1)$$

Here, $\mu_0$ designates the central ($r = 0$) surface brightness, $r_0$ is the scalelength of the profile and $N$ is the Sérsic index. Because of its simpler mathematical dependence on the free parameters, we decided to use the above formula instead of

$$\mu(r) = \mu_{\rm eff} + 1.0857 b_n \left[\left(\frac{r}{r_{\rm eff}}\right)^{1/n} - 1\right], \quad (2)$$

where $b_n \approx 1.9992n - 0.3271$ for $0.5 < n < 10$ (Graham & Worley 2008, and references therein). There are simple relations between the quantities involved in both equations (e.g. MacArthur, Courteau & Holtzman 2003):

$$n = 1/N \quad (3)$$

$$\mu_{\rm eff} = \mu_0 + 1.0857 b_n \quad (4)$$

$$r_{\rm eff} = r_0 b_n^n, \quad (5)$$

which allow us to easily obtain the effective radius ($r_{\rm eff}$) and the surface brightness at this radius ($\mu_{\rm eff}$) from the parameters of equation (1). Following the results of the numerical simulations performed by Gavazzi et al. (2005), it was decided not to correct the Sérsic parameters for seeing effects (Trujillo et al. 2001a,b) unless a Sérsic index $n$ greater than 3 was obtained.

The structural parameters obtained from the fits are listed in Table 2. The profile fits and their residuals $\Delta\mu = \mu({\rm obs}) - \mu({\rm fit})$ are plotted in Fig. 3.

#### *3.2.1 FS90 110*

As mentioned in Section 2.2, the centre of FS90 110 is overexposed in the *R* long-exposure image obtained with MOSAIC. Thus, we

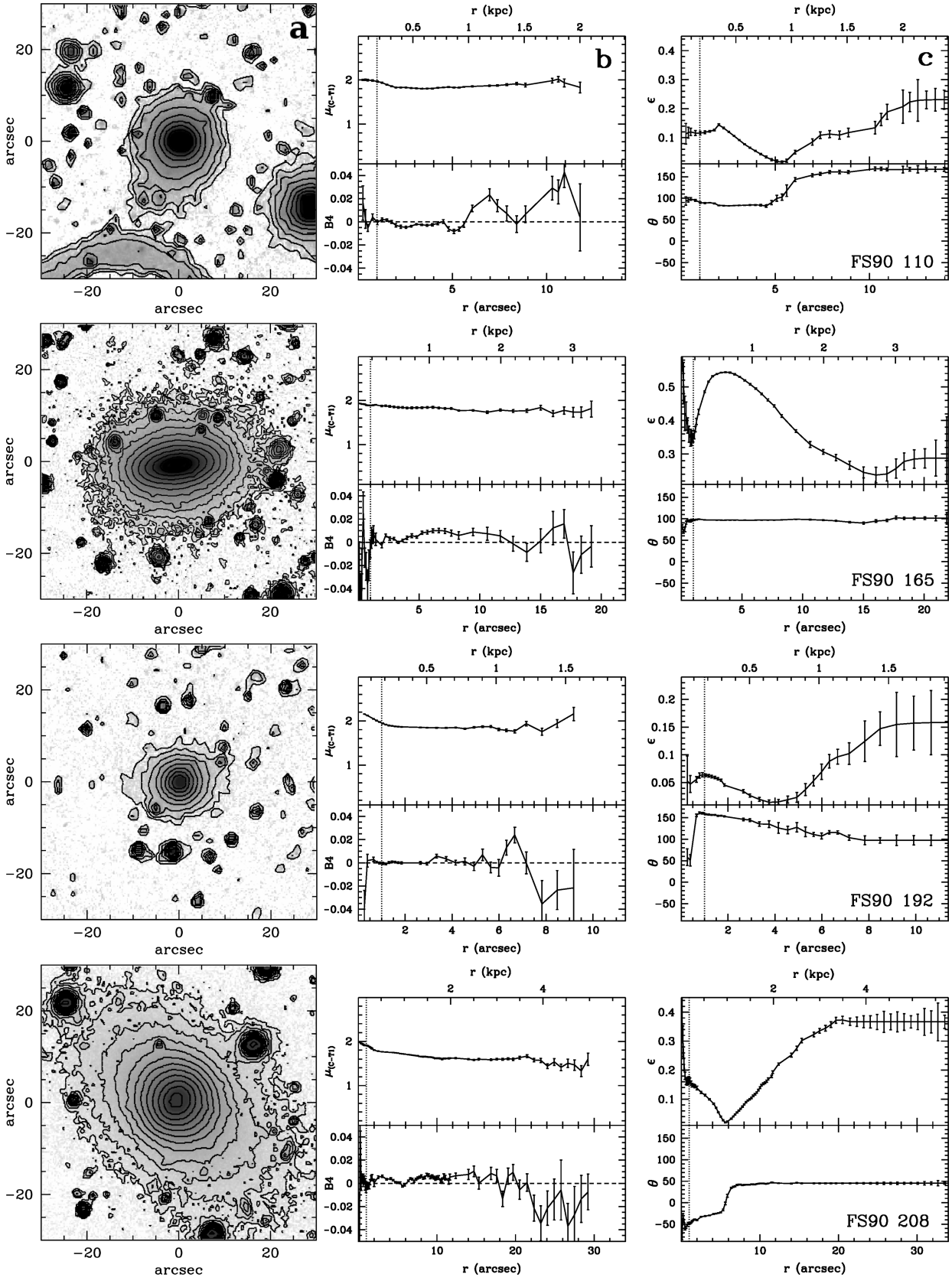


**Figure 2.** FS90 cE candidates located in the central region of the Antlia cluster. From top to bottom: FS90 110, FS90 165, FS90 192 and FS90 208. From left to right. (a) Brightness contour levels superimposed on the *R* images of the galaxies. At the adopted Antlia distance, 1 arcsec $\simeq$ 170 pc. North is up and east is to the left. (b) $(C - T_1)$ colour profiles reddening corrected (top) and ELLIPSE B4 index (bottom) against equivalent radius. (c) Ellipticity ($\epsilon$, top) and position angle ($\theta$, bottom) against equivalent radius. Positive angles are measured from north to east. The vertical dotted lines in (b) and (c) show the region of seeing influence. The equivalent radius scale displayed at the top of the panels in (b) and (c) was obtained with the assumed Antlia distance.

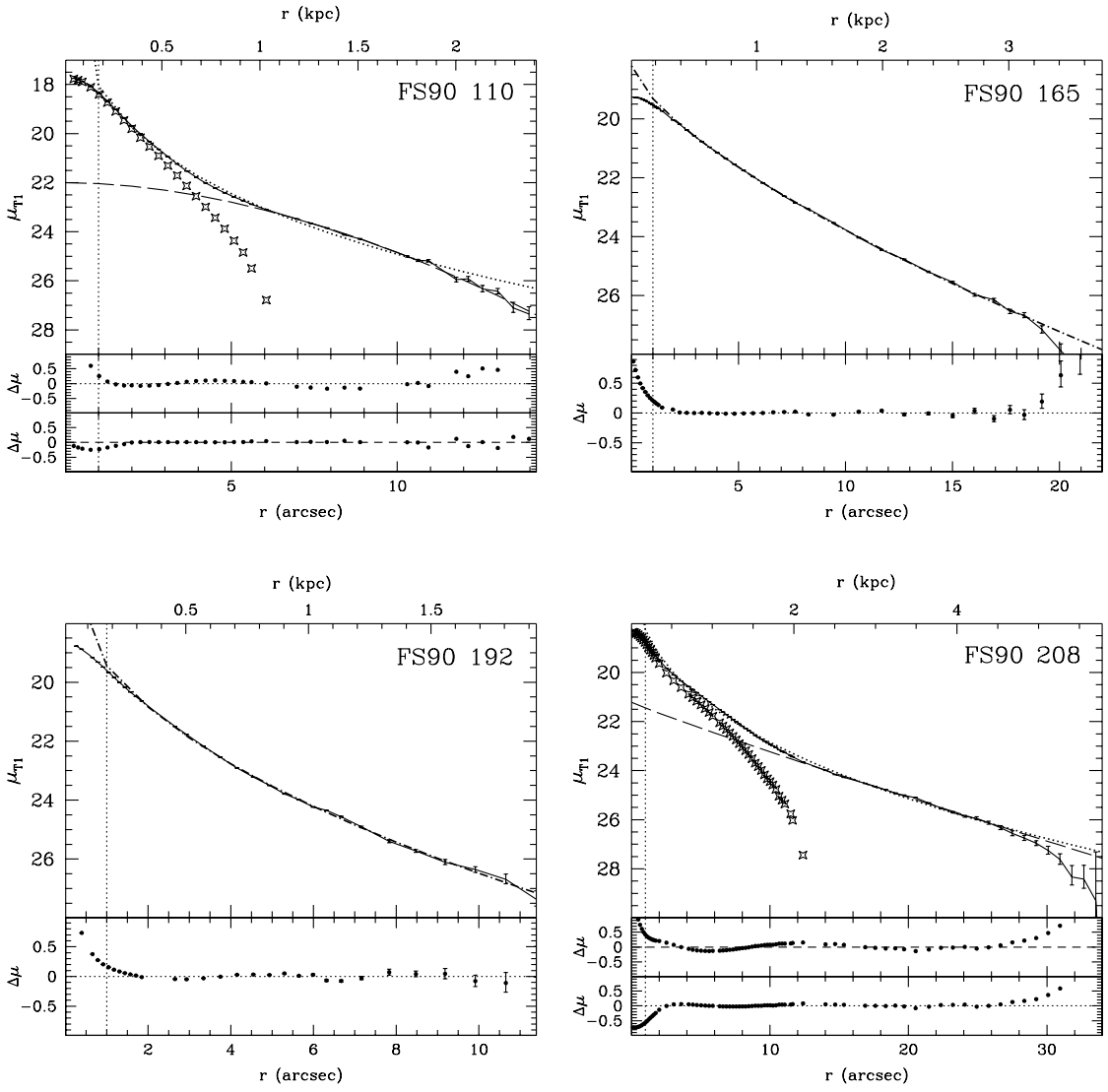


**Figure 3.** Fits of the Sérsic law to the absorption corrected $T_1$ brightness profiles of the FS90 cE candidates located in the central region of Antlia. The residuals $\Delta\mu = \mu(\text{obs}) - \mu(\text{fit})$ are shown in the lower panels. For FS90 110 and FS90 208, which display two-component profiles, the upper residuals correspond to the fit of a single Sérsic law (dotted curve), and the lower ones to a two-component fit. For clarity, in these cases we only show the Sérsic fit for the outer component (dashed line), which is subtracted to show the inner component (open symbols). The equivalent radius scale at the top of the four panels was obtained from the adopted Antlia distance (1 arcsec $\simeq$ 170 pc).

**Table 2.** Structural parameters of FS90 cE candidates, obtained from different fits of the Sérsic law to their absorption corrected $T_1$ brightness profiles. $r_{\rm int}$ and $r_{\rm ext}$ refer to the inner and outer equivalent radius considered for the fits, respectively. $T_1$ gives the integrated magnitude obtained from the fitted Sérsic profile.

| Object | Component | $r_{\rm int}$ (arcsec) | $r_{\rm ext}$ (arcsec) | $\mu_0$ (mag arcsec$^{-2}$) | $r_0$ (arcsec) | $N$ | $\mu_{\rm eff}$ (mag arcsec$^{-2}$) | $r_{\rm eff}$ (arcsec) | $n$ | $T_1$ |
|---|---|---|---|---|---|---|---|---|---|---|
| FS90 110 | Inner | 2.3 | 4.8 | $17.73 \pm 0.02$ | $1.17 \pm 0.01$ | $1.23 \pm 0.01$ | 19.13 | 1.43 | 0.81 | 15.61 |
| FS90 110 | Outer | 6.0 | 11.8 | $21.99 \pm 0.45$ | $6.07 \pm 2.78$ | $1.83 \pm 0.36$ | 22.82 | 5.26 | 0.55 | 16.84 |
| FS90 165 | Single | 2.2 | 13.8 | $18.19 \pm 0.06$ | $0.94 \pm 0.05$ | $0.69 \pm 0.01$ | 20.98 | 3.69 | 1.45 | 15.25 |
| FS90 192 | Single | 1.6 | 9.9 | $15.77 \pm 0.34$ | $0.07 \pm 0.02$ | $0.46 \pm 0.02$ | 20.12 | 1.42 | 2.17 | 16.27 |
| FS90 208 | Inner | 2.0 | 9.8 | $19.14 \pm 0.08$ | $2.92 \pm 0.29$ | $1.29 \pm 0.04$ | 20.44 | 3.37 | 0.77 | 15.04 |
| FS90 208 | Outer | 12.4 | 24.9 | $21.21 \pm 0.55$ | $5.26 \pm 2.45$ | $0.93 \pm 0.14$ | 23.16 | 9.90 | 1.07 | 15.52 |

used the short-exposure image to obtain its inner brightness profile up to an equivalent radius of $r = 1.8$ arcsec. For larger radii, we used the *R* long-exposure frame to obtain its brightness profile out to $r \sim 14$ arcsec ($\mu_{T_1} = 27.5$ mag arcsec$^{-2}$), starting with the parameters for $r = 1.8$ arcsec.

The centre of the elliptical apertures, the ellipticity $\epsilon$ and the position angle $\theta$ were allowed to vary freely for the inner fit. For the outer fit, they were fixed once the convergence of the isophotal fit was prevented because of the low surface brightness of the outermost isophote.

The ellipticity shows a strong variation on a small radial scale. It changes from $\epsilon = 0.14$ at $r \sim 2$ arcsec, to $\epsilon = 0.01$ at $r = 5.3$ arcsec. Then, it increases up to $\epsilon = 0.22$ at $r = 12.3$ arcsec and after that it remains constant. This behaviour is followed by the position angle as it varies from $\theta \sim 83^\circ$ in the range $r = 2$–4.5 arcsec, to $\theta \sim 160^\circ$ at $r \sim 8$ arcsec. The B4 coefficient becomes positive (i.e. discy isophotes) in the outer region, at a similar radius as that for which the ellipticity and the position angle change in a significant manner.

The outer isophotes of FS90 110 display an elongation towards NGC 3258 in the *R* MOSAIC image, as can be seen from Fig. 2. Therefore, we performed several isophotal fits to test whether the strong variations in position angle and ellipticity could be an artefact due to the presence of this low surface brightness structure. We performed an outer fit, keeping the position of the centre fixed during the whole process, and an outer fit masking half of the galaxy in the direction to NGC 3258. In all these cases, $\theta$ and $\epsilon$ show, within the errors, the same behaviour as in the free isophotal fit.

The colour profile of this galaxy does not show any perceptible gradient out of the region of seeing influence.

We performed several fits of the Sérsic law to the $T_1$ brightness profile of FS90 110. It was found that it is more convenient to fit the profile with two components, as a single-component fit gives systematic positive and negative residuals (see Fig. 3). Furthermore, variations of the range in equivalent radius used to perform single-component fits make the Sérsic index *N* evolve from convex profiles for larger ranges to concave profiles for smaller intervals.

Following Cellone & Buzzoni (2001), to obtain possible analytical profiles for the two components, we first fitted a Sérsic law to the outer region of the galaxy in the range $r = 6.0$–11.8 arcsec (dashed line in FS90 110 panel of Fig. 3). Then, we subtracted the intensities of this model from those observed in the whole profile range. In this way, we recovered the inner component (open symbols in Fig. 3), which was then fitted with an independent Sérsic law (not shown in Fig. 3 for clarity).

We are aware that this decomposition scheme might not be unique as it depends on the radial ranges selected to perform the fits, as well as on sky subtraction effects (see, for instance, Cellone & Buzzoni 2001, for a discussion about the art of profile fitting). However, the validity of our approach is supported by the small and stable residuals shown in Fig. 3. Moreover, a fit of two coupled general Sérsic laws to the profile of FS90 110 in the range 2.3–11.8 arcsec has given structural parameters that are in agreement, within the errors, with those given in Table 3.

The integrated magnitudes obtained for both components from their individual Sérsic fits show that the inner component could be $\sim$ three times brighter than the outer component, making this galaxy a bulge-dominated system. It is worth noting that the radius at which the changes in ellipticity and position angle arise is similar to that at which the outer component seems to begin to dominate the brightness profile.

### 3.2.2 FS90 165 (confirmed Antlia member)

The fit of elliptical apertures in the central region of FS90 165 was performed on the short-exposure *R* image, as its centre is overexposed in the long-exposure image. The inner profile was obtained by allowing the centre, ellipticity and position angle to vary freely. The fit reaches an equivalent radius of $r \sim 1.4$ arcsec, and from this radius outwards, we worked with the long-exposure *R* image to obtain an outer profile reaching $r \sim 19.2$ arcsec ($\mu_{T_1} = 27.3$ mag arcsec$^{-2}$).

Again, we allowed for free variation of all elliptical apertures parameters until the outermost (low surface brightness) regions of the galaxies were reached.

The ellipticity shows an almost constant value of about $\epsilon = 0.53$ from $r \sim 2$ arcsec to $r \sim 4$ arcsec, and then displays a smooth decrease until $\epsilon = 0.23$ at $r \sim 16$ arcsec. The position angle has a constant value of $\theta \sim 100^\circ$ along the whole profile. This behaviour of the elliptical apertures can be seen in Fig. 2(a): the ellipses become more and more elongated towards the centre, while their orientation has no detectable variation. The B4 coefficient is positive over the whole equivalent radius range, showing that the isophotes of this galaxy are discy.

Outside $r = 2$ arcsec, the colour profile displays a slight blue gradient of $\sim 0.1$ mag, from $(C - T_1)_0 = 1.87$ at $r = 2.25$ arcsec, to $(C - T_1)_0 = 1.76$ at $r = 13.8$ arcsec.

The brightness profile was fitted by a single Sérsic law in the range $r \sim 2$– 14 arcsec. The analytical profile is shallower than a de Vaucouleurs law, and the effective radius obtained from it is in good agreement with that measured from the observed profile (see Table 2).

### 3.2.3 FS90 192

As the centre of this galaxy is not overexposed in the long-exposure frames, the fit of elliptical apertures was performed on the long-exposure *R* image up to an equivalent radius of $r \sim 11.4$ arcsec ($\mu_{T_1} = 27.6$ mag arcsec$^{-2}$). The centre of the ellipses, the isophotal ellipticity and position angle were allowed to vary freely, until the low surface brightness of the outermost regions prevented a good convergence of the fits.

The ellipticity is consistent with circular isophotes out to $r \sim 5$ arcsec, and then it begins to increase smoothly until it reaches a

**Table 3.** Data adopted for the confirmed cE galaxies plotted in Fig. 5. In all cases, the mean effective surface brightness ($\langle\mu_{\rm eff}\rangle$) was obtained from the effective radius ($r_{\rm eff}$), and *R* magnitudes transformed into $T_1$ magnitudes using $R - T_1 = -0.02$ (see Section 2.1), with equation (1) of Paper I. For A496cE, the *R* magnitude was calculated from its $r'$ magnitudes (Chilingarian et al. 2008), using $(r' - R_{\rm c}) = 0.25$ (Fukugita et al. 1995).

| Galaxy | $E(B-V)$ (mag) | $(m-M)$ (mag) | Dist. (Mpc) | $R$ (mag) | $r_{\rm eff}$ (arcsec) | $\langle\mu_{\rm eff}\rangle$ (mag arcsec$^{-2}$) | $r_{\rm tot}$ (kpc) | Companion | Dist. comp. (kpc) | References |
|---|---|---|---|---|---|---|---|---|---|---|
| M32 | 0.062 | 24.53 | 0.8 | 7.68 | 28.5 | 16.9 | 1.2 | M31 | 5.5 | 1,2,3 |
| NGC 4486B | 0.021 | 31.26 | 17.9 | 12.72 | 2.5 | 16.7 | 1.0 | NGC 4486 | 28 | 4,5,6 |
| NGC 5486A | 0.055 | 32.08 | 26.1 | 13.07 | 4.1 | 18.1 | 1.6 | NGC 5486 | 3.1 | 6,7,8 |
| A496cE | 0.138 | 35.70 | 138.0 | 17.35 | 0.7 | 18.6 | – | A496 cD | 14 | 9 |

Extinction values are from Schlegel et al. (1998). References: (1) Mateo (1998) and references therein; (2) Graham (2002); (3) Choi et al. (2002); (4) Alonso et al. (2003); (5) Tonry et al. (2001); (6) Nieto & Prugniel (1987); (7) Mahdavi et al. (2005); (8) de Vaucouleurs et al. (1991); (9) Chilingarian et al. (2008).

maximum value of $\epsilon = 0.16$ in the outer regions. The position angle shows a smooth decrease of 60° from the innermost isophotes (out of the seeing influence region) to the outermost ones.

There is no perceptible gradient in the $(C - T_1)$ colour profile, except that seen at $r < 2$ arcsec, likely a result of seeing effects.

The brightness profile was successfully fitted by a single Sérsic profile in the range $r \sim 2$–10 arcsec. This galaxy does not follow a de Vaucouleurs law, but a shallower one. However, we should stress that we do not have a radial velocity for this object. If it was a background galaxy, we would likely lose the central steepening of the profile because of seeing and distance effects.

The effective radius obtained from the analytical profile is in good agreement with that calculated from the observed profile.

#### *3.2.4 FS90 208 (confirmed Antlia member)*

The short-exposure *R* image was used to obtain an inner profile up to $r = 2$ arcsec. The rest of the profile was obtained from the long-exposure frame, up to $r = 30.1$ arcsec ($\mu_{T_1} = 27.5$ mag arcsec$^{-2}$). Once more, all the elliptical parameters were allowed to vary freely, until a good convergence was prevented because of the low surface brightness of the outer isophotes.

This galaxy presents a remarkable change both in ellipticity and in position angle at $r = 5.6$ arcsec. The ellipticity decreases from $\epsilon = 0.14$ at $r = 2$ arcsec, to $\epsilon = 0.02$ at $r = 5.6$ arcsec, and then increases to $\epsilon = 0.37$ at $r = 23.2$ arcsec. From this point outwards, the ellipticity remains constant. The position angle follows the changes in ellipticity, as it varies from $\theta = -22°$ at $r = 5$ arcsec, to $\theta = 41°$ at $r = 7$ arcsec, and then it remains more or less constant. These variations are similar to those displayed by FS90 110, albeit stronger. The B4 coefficient for this galaxy is consistent with its isophotes being discy.

A small colour gradient is present in the $(C - T_1)$ profile. The colour becomes bluer outwards, from $(C - T_1) = 1.8$ at $r = 2$ arcsec, to $(C - T_1) = 1.6$ at $r = 10$ arcsec. From this point to the outskirts of the galaxy, the colour remains constant.

As in the case of FS90 110, the brightness profile of FS90 208 is better fitted by two components for the same reasons. Therefore, we fitted a Sérsic profile to the outer part of the galaxy, in the range $r = 12.4$– 24.9 arcsec, which was then subtracted in intensities from the original profile. We then recovered the inner component and fitted an independent Sérsic law to it (see Fig. 3).

From the integrated $T_1$ magnitudes of both components, we found that the inner component seems to be not so prominent in comparison with the outer component, as the former is ∼1.6 times brighter than the latter. In contrast to FS90 110, the radius at which the changes in ellipticity and position angle arise is smaller than that found to possibly separate the two components.

### 3.3 Colour maps and unsharp masking

In order to obtain information about the internal structure of the FS90 cE candidates, we built colour maps with their *R* and *C* short- and long-exposure images. The individual images were previously filtered by applying a median filter with a window size of 5 × 5 pixel to reduce the noise of the maps.

Following Lisker et al. (2006b), we have also performed an unsharp masking process on the long-exposure *C* images of the four galaxies. The *C* frames were used instead of the *R* frames, as none of the galaxy centres is overexposed in the *C* frames. We have produced circular and elliptical masks, considering Gaussian kernels with $\sigma$ values in the range 3–30 pixel (i.e. 0.8–8 arcsec). To build the elliptical masks, we used the position angles and ellipticities of the outer isophotes of each galaxy.

In addition, to test the existence of hidden discs, we have analysed the residual images obtained from a fixed ELLIPSE fitting (i.e. by fixing the position angle and ellipticity in the whole fitting process).

For FS90 110 and FS90 192 we have found no evidence of internal structure. Both colour maps are smooth and show redder centres than the outskirts, in agreement to what is seen in their colour profiles (see Fig. 2). As there are FORS1 and ACS images available for these, we continue this analysis in Section 4.2.

Fig. 4 shows, for FS90 165 and FS90 208, $(C - T_1)$ colour maps and resulting images of the unsharp masking process. It can be seen that the mask of FS90 165 shows a red disc-like structure, not evident in its colour profile. This structure is in agreement with the existence of discy isophotes, as expected from the positive values of the B4 index (see Fig. 2). FS90 165 seems to be a low-luminosity lenticular galaxy, displaying a similar colour map to those of similar objects (see, for example, Chilingarian et al. 2008).

The colour map of FS90 208 is smooth with a small red gradient towards the centre, also evident in its colour profile. In contrast, the unsharp mask performed using an elliptical kernel with the same ellipticity and position angle of its outer component shows a possible bar-like structure, which seems to be present in the residual image of a fixed ELLIPSE fitting (not shown).

### 3.4 Colour–magnitude and luminosity versus mean effective surface brightness relations

The left panel of Fig. 5 shows a $T_1$ versus $\langle\mu_{\rm eff}\rangle$ (absorption corrected) plot for the FS90 early-type galaxies from our sample of Paper I, where the FS90 morphology has been indicated. We also depict, as a reference, the locus of constant effective radius followed by galaxies fainter than $T_1 = 13$ mag (see Paper I). In this plot, the locations of all these galaxies correspond to observed apparent magnitudes. For comparison, we have also included some confirmed cE galaxies that display the positions they would have at the Antlia distance. These are M32 (large solid pentagon), NGC 4486B (large open triangle), NGC 5846A (large star) and A496cE (large asterisk); see Table 3.

In this figure, FS90 165 and FS90 208 share the locus of the Antlia early-type galaxies. In contrast, FS90 110 and FS90 192 are located far from this relation defined by early-type galaxies, towards higher mean effective surface brightness, smaller effective radius or fainter magnitudes.

In particular, FS90 110 presents the highest mean effective surface brightness of the whole sample from Paper I, with the exception of FS90 94, a bright S0 Antlia member. Furthermore, FS90 110 seems to extend the sequence followed by bright elliptical and S0 galaxies (in a perpendicular direction with respect to the relation of early-type galaxies), in the same way as M32 would do if it were placed at the Antlia distance. This latter correlation corresponds to the Kormendy (1977) scaling relation followed by bright ellipticals and bulges of spiral galaxies on the $r_{\rm eff}$–$\mu_{\rm eff}$ plot, which is a projection of the Fundamental Plane (Djorgovski & Davis 1987). NGC 4486B and NGC 5846A and A496cE are also located within this sequence, towards smaller effective radius. However, M32 is the most extreme case. This behaviour of cE galaxies has already been noticed by, for instance, Nieto & Prugniel (1987); see also Chilingarian et al. (2007). FS90 192 does not follow the same trend as cEs.

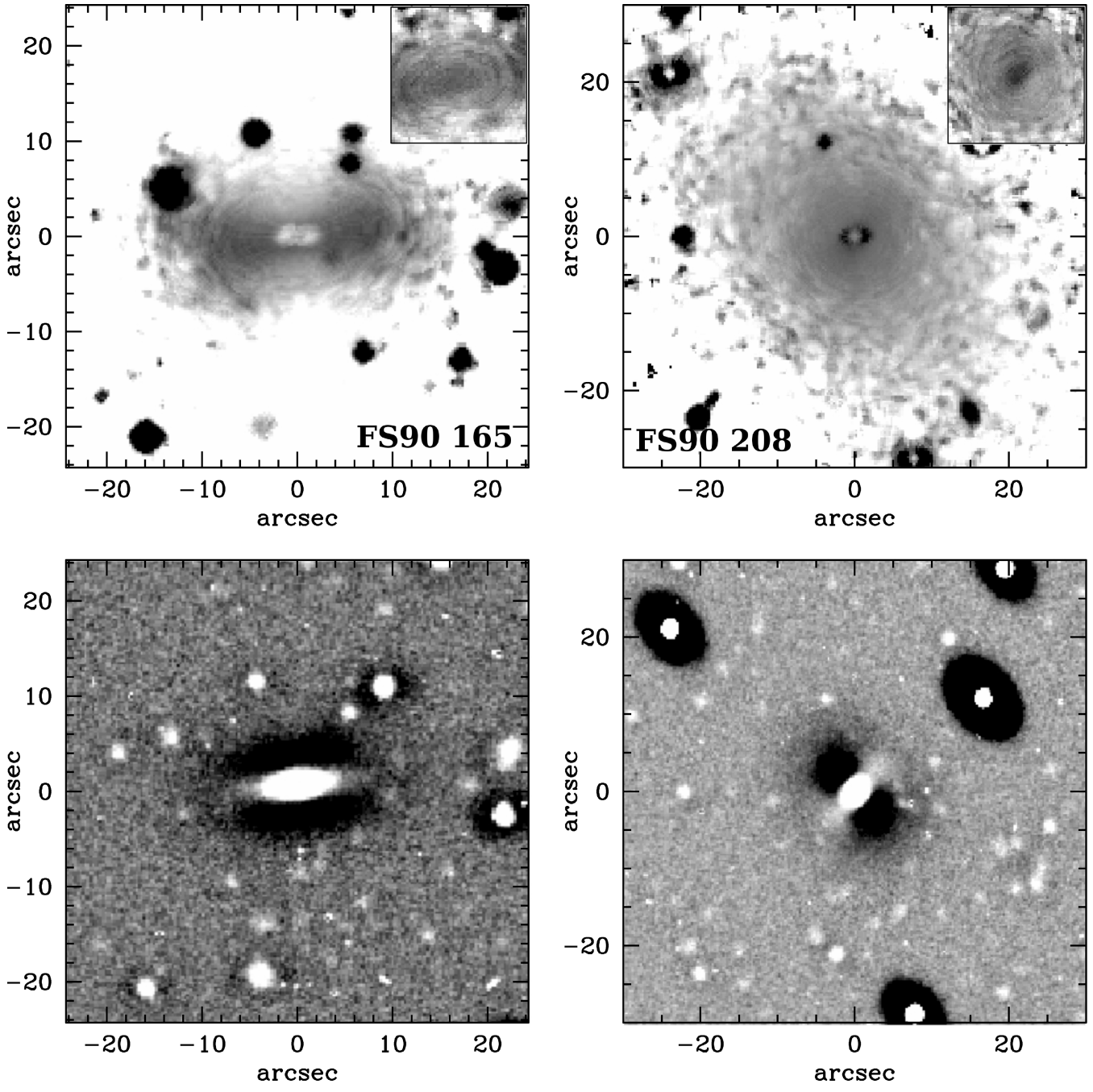


**Figure 4.** Top: $(C - T_1)$ colour maps of FS90 165 and FS90 208. The large maps were obtained from long-exposure images, and the small maps, in the upper-right corners, from short-exposure frames to recover the overexposed central region. The linear scale of the small colour maps is the same as in the large maps. A median filter with a window size of 5 × 5 pixel was applied to all individual images, previous to the construction of the maps. The greyscale corresponds to a colour range $(C - T_1) = 0.0$–3.0 mag, in which black refers to red colours, and white to blue colours. Bottom: elliptical unsharp masks with kernel size $\sigma = 7$ pixel of FS90 165 (left) and FS90 208 (right).

The right panel of Fig. 5 shows the colour–magnitude diagram of the FS90 early-type galaxies from the sample of Paper I, where the FS90 cE candidates have been included. The solid line shows the mean colour–magnitude relation followed by early-type Antlia galaxies. It can be seen that FS90 110 is located on the red border of the relation, at almost the same position as FS90 165, and evidently separated from the early-type background galaxies with similar apparent magnitudes. In contrast, FS90 192 clearly deviates from the colour–magnitude relation of Antlia members towards redder colours, or fainter magnitudes.

We note that, considering the $(B - R)$ versus $M_B$ colour–magnitude relation of the Perseus cluster (Conselice, Gallagher & Wyse 2002), and adopting for M32 $(B - R) \sim 1.45$ mag (Peletier 1993) and $M_R \sim -16.8$ (see Table 3), the location of M32 in this

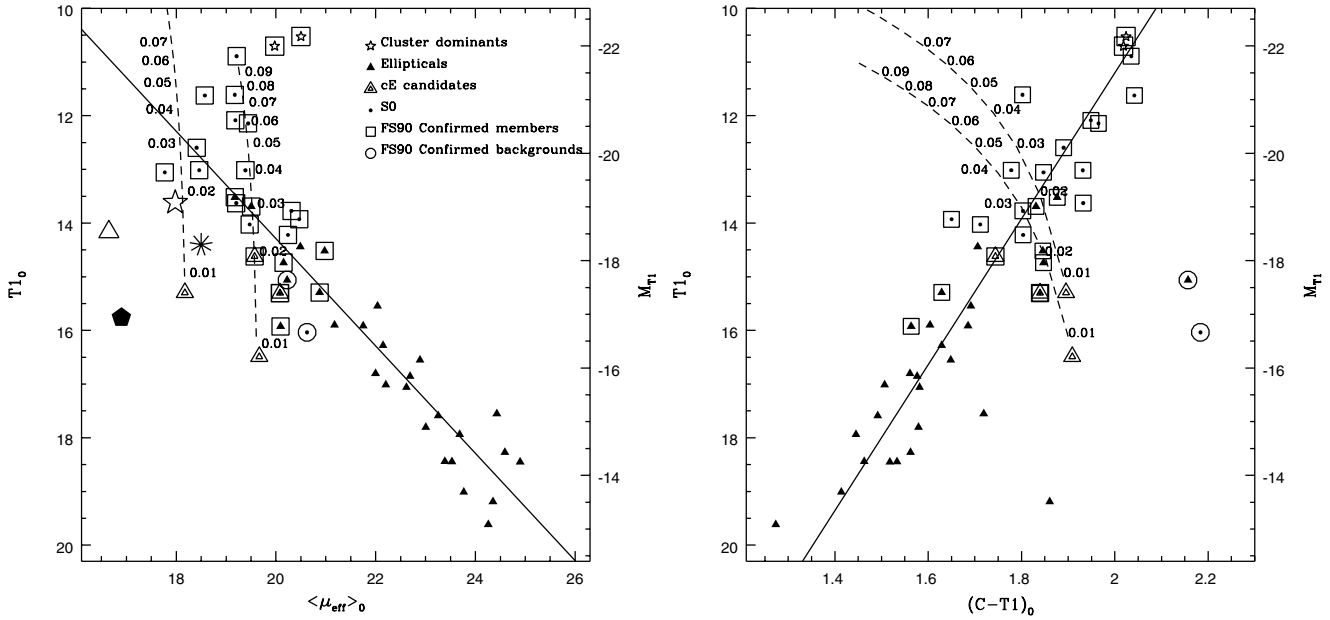


**Figure 5.** Left: $T_1$ magnitude versus mean effective surface brightness plot where different morphologies are indicated. The solid line is the locus of constant effective radius ($\sim$ 1 kpc) of Antlia early-type galaxies with $T_1 > 13$ mag (see Paper I). Two FS90 cE candidates set the lowest limit in effective radii of our sample from Paper I. All galaxy positions in the plot correspond to their observed apparent magnitudes, except for M32 (large solid pentagon), NGC 4486B (large open triangle), NGC 5846A (large star) and A496cE (large asterisk), which show the location they would display if they were at the Antlia distance. The dashed lines show the possible locations that FS90 110 and FS90 192 would hold at the Antlia distance, if their true distances corresponded to the redshift range $z = 0.01$–$0.1$ (small numbers close to the dashed lines indicate such redshifts). Right: colour–magnitude diagram including the FS90 cE candidates (symbols as in the left panel). The solid line shows the mean colour–magnitude relation followed by early-type Antlia galaxies (Paper I). The dashed lines correspond to those displayed in the left panel. The absolute magnitude scale (on the right of both panels) is only valid for Antlia confirmed members.

diagram presents the same trend as FS90 110 and FS90 192 in ours (i.e. shifted towards redder colours or fainter magnitudes from the cluster mean colour–magnitude relation).

As an additional test, we assume that FS90 110 and FS90 192 are elliptical background galaxies that 'fall off' the mean relations followed by Antlia early-type members, because of the effect of distance. Then we can calculate the shift of their positions in the $\langle\mu_{\rm eff}\rangle$ versus $r_{\rm eff}$ and colour–magnitude plots applying cosmological dimming and *K*-corrections to their observed surface brightnesses, and luminosities and colours, respectively. From Fukugita, Shimasaku & Ichikawa (1995), we adopt the *K*-correction to $(B - R)$ for an elliptical galaxy. Assuming that early-type galaxies are old stellar systems, we transformed this correction into $(C - T_1)$ following Forbes & Forte (2001). The dashed lines in both panels of Fig. 5 show the different positions that these galaxies would hold at the Antlia distance, if their real distances were within a redshift range $z = 0.01$–$0.1$. Please note that a redshift of $z \approx 0.01$ corresponds approximately to the adopted Antlia distance.

Fig. 5 shows that, to fall on the locus of the Antlia relation, FS90 110 might have, at most, an intrinsic luminosity similar to those of bright early-type Antlia members, then being at a distance of $\sim$120 Mpc ($z \approx 0.03$). This shift would place it within the colour–magnitude relation in the right panel.

For FS90 192, two options exist in the $\langle\mu_{\rm eff}\rangle$ versus $r_{\rm eff}$ plot: it could be a bright dwarf elliptical at $\sim$120 Mpc, or a giant elliptical galaxy placed as far as $\sim$400 Mpc ($z \approx 0.1$). However, from the colour–magnitude diagram, we can see that the second possibility must be discarded as, for that redshift, FS90 192 would be completely out of the mean relation.

Regarding FS90 192, the images do not show any concentration of galaxies in its neighbourhood, which would make it an interesting object even if it were not confirmed as an Antlia cE galaxy; isolated ellipticals of moderate luminosity are not common objects. In the case of FS90 110, we cannot rule out from the present analysis that it may be an ordinary background galaxy.

## 4 ANALYSIS OF FORS1 AND ACS DATA

In order to obtain more evidence in favour of, or against, FS90 110 and FS90 192 being cE galaxies, we have analysed two frames obtained with FORS1, centred on NGC 3258 and NGC 3268, respectively. As mentioned above, these frames are deeper and were taken under better seeing conditions than the MOSAIC frames. We have also used two ACS images from the *HST* archive also centred on NGC 3258 and NGC 3268, respectively. Unfortunately, there are no similar data available for FS90 165 and FS90 208.

### 4.1 Low surface brightness bridge

In the FORS1 and ACS images of FS90 110 and FS90 192, we have not detected outer structures different from those previously seen on the MOSAIC images. The very low surface brightness 'bridge' that seems to link FS90 110 to NGC 3258 is detected in both the *V* and *I* FORS1 images as well as in the F814W ACS frame. No comparable structures were found in the corresponding images of FS90 192. Its outer isophotes look regular without visible evidence of distortion.

In the top panel of Fig. 6, we show brightness contour levels superimposed on the F814W ACS frame of FS90 110 from which a model of NGC 3258 has been subtracted. In order to test whether the low surface brightness structure could be just an artefact due to the subtraction of NGC 3258, we added to the original *V* FORS1

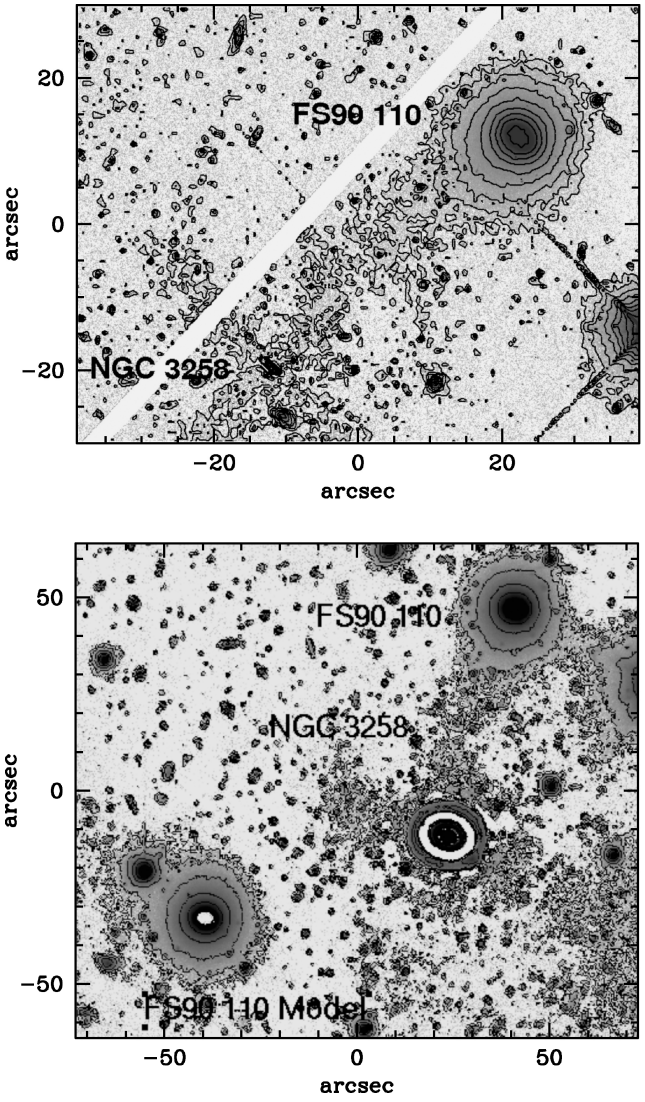


**Figure 6.** Contour maps showing the low surface brightness structure that seems to link FS90 110 to NGC 3258. Top: F814W ACS frame from which a model of NGC 3258 has been subtracted. Bottom: to test whether the low surface brightness 'bridge' is an artefact due to the subtraction of the light of NGC 3258, we have added a model of FS90 110 to the *V* FORS1 image, shifted in position angle from its original location but keeping its galactocentric distance to the centre of the dominant galaxy. After the subtraction of the NGC 3258 light model, there is no similar low surface brightness structure left around the artificial FS90 110 galaxy.

image of NGC 3258 a model of FS90 110 obtained with BMODEL. This artificial galaxy with similar characteristics as FS90 110, was placed in a different position but keeping the original galactocentric distance to the centre of the dominant galaxy. We subtracted the light of NGC 3258 from this new image, and no low surface brightness 'bridge' was found at the location of the added object (see Fig. 6). This result can be understood as proof that such a 'bridge' is not a spurious detection as a result of image processing. Another argument supporting this statement is the fact that this low surface brightness structure does not connect the two galaxy centres, as can be seen in both panels of Fig. 6.

### 4.2 Colour maps and unsharp masking

With the aim of obtaining additional information on the possible internal structure of FS90 110 and FS90 192, we built $(V - I)$ and $(B - I)$ colour maps from the FORS1 and ACS images, respectively. We have also performed unsharp masking on these frames with the best signal-to-noise ratio (i.e. the FORS1 *V* and ACS *I* images). Elliptical masks were constructed in a similar way as those of MOSAIC.

Fig. 7 shows the ACS $(B - I)$ colour map of FS90 110 (left panel), which has a better spatial resolution than that of FORS1. A FORS1 unsharp elliptical mask is also displayed (right panel), resulting from a $\sigma$ value of 5 pixel (i.e. 1 arcsec). In the inner region of FS90 110, we see an embedded warped structure, which is detected on both the colour map and the mask. This structure is redder than the rest of the galaxy.

Although the ACS images show a higher spatial resolution, we prefer to show a FORS1 mask, as the former contains an artefact in the same location where the inner structure is expected to show up. All bright point sources also show this artefact (note the bright star at the right side of the top panel of Fig. 6.)

In the colour maps and unsharp masks of FS90 192 (not shown), we have not found any structure different from what has been already seen in the MOSAIC data.

### 4.3 Brightness profiles

Fig. 8 shows a comparison of the MOSAIC $T_1$ brightness profiles of FS90 110 and FS90 192, with the *V* and *I* profiles obtained from FORS1 and ACS, respectively. The photometric parameters obtained from the VLT *V* and *I* profiles are listed in Table 4.

Most of the features observed in the MOSAIC profiles are confirmed through VLT and *HST* images, including the ellipticity and position angle variations. The exception is the ELLIPSE B4 coefficient behaviour in FS90 110, as it does not become positive at $r \sim 6$ arcsec. The high central surface brightness displayed by FS90 110 in the ACS profile is noticeable, detected thanks to the low FWHM of these images.

In order to test the values of the *N* Sérsic indices obtained for the $T_1$ brightness profile (see Section 3.2) of FS90 110, we have fitted two coupled general Sérsic laws to its ACS *I* brightness profile, within the equivalent radius range 2.0–11.8 arcsec. The Sérsic indices *N* (i.e. $1/n$) for both components resulting from this new fit ($1.8 \pm 0.2$ and $1.25 \pm 0.05$ for the outer and inner components, respectively) are in good agreement with those obtained from the MOSAIC profile (see Table 2).

We intended to perform a two-component fit over the whole useful range of the ACS profile (i.e. 0.3–11.8 arcsec), as the innermost 0.3 arcsec are expected to be affected by the seeing. However, no model could be obtained that properly fitted the whole profile considering an inner cut radius lower than 1.5 arcsec (>2 FWHM). This indicates that two Sérsic laws can represent the light profile of the galaxy only if the central region is excluded from the fit. Such a limitation of Sérsic profiles could not be avoided by, for example, performing a point spread function (PSF) convolution with the model.

Choi et al. (2002) have obtained the *I* profile of M32, which is shown in Fig. 8 with its equivalent radius rescaled to the Antlia distance. In addition, we have obtained the ACS *z* profile of NGC 4486B, which is also shown rescaled. The profiles of FS90 110 and M32 look similar in both shape and high central surface brightness, although the former extends over a larger galactocentric

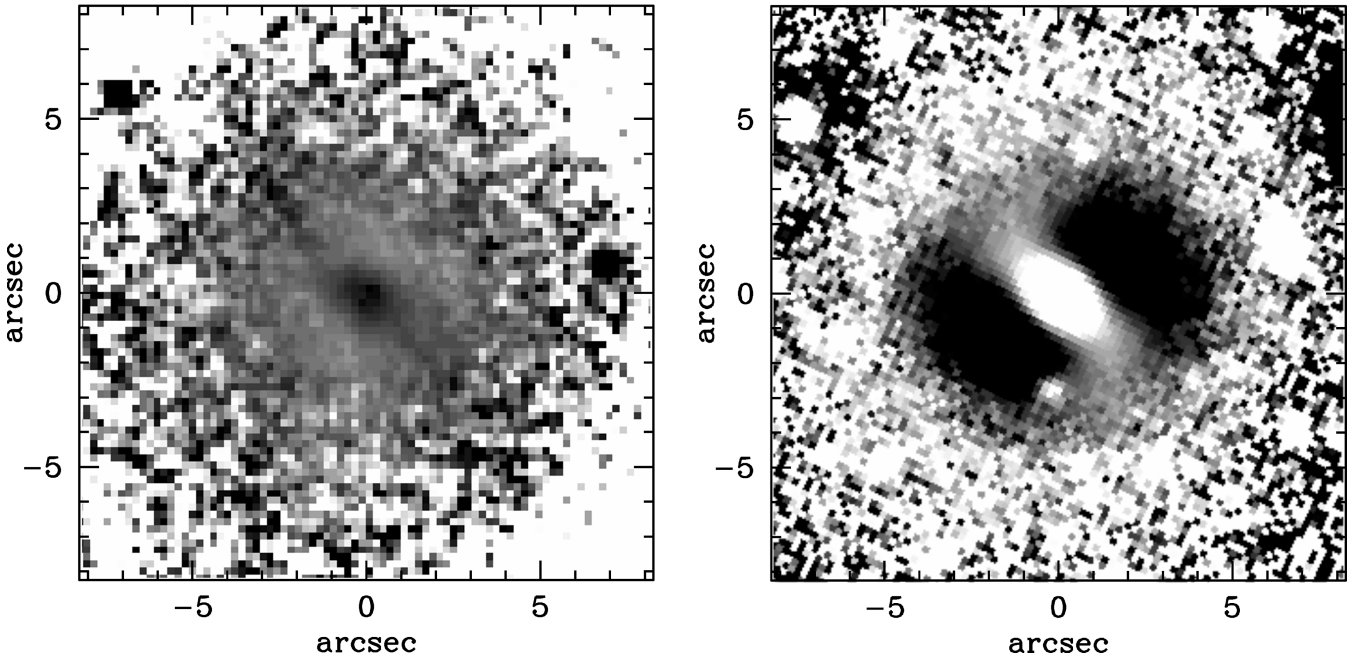


**Figure 7.** Left: $(B - I)$ colour map of FS90 110, obtained from ACS images. A median filter with a window size of $5 \times 5$ pixel was applied. The displayed greyscale corresponds to a colour range $(B - I) = 0.0$–$2.5$ mag, in which black refers to red colours and white to blue colours. Right: FS90 110 FORS1 elliptical unsharp mask, obtained with a Gaussian kernel size of $\sigma = 5$ pixel (i.e. 1 arcsec).

radius. M32 also displays significant changes in both ellipticity and position angle (Choi et al. 2002), similar to those found in FS90 110. However, NGC 4486B is larger than FS90 110 and does not show a two-component profile, similar to FS90 192. This is in agreement with Ferrarese et al. (2006), who fitted a single-component Sérsic law to the profile of NGC 4486B.

## 5 DISCUSSION AND CONCLUSIONS

### 5.1 FS90 165

From the analysis performed in the previous section, we conclude that FS90 165, a spectroscopically confirmed Antlia member, cannot be considered as a cE galaxy. It follows the fundamental relations of low surface brightness early-type Antlia galaxies (see also Paper I), is larger than any confirmed cE object and presents no compact morphology. It is also located far away in projection from any bright galaxy, and from the central cluster region, a characteristic shared by all confirmed cE galaxies. Its $T_1$ brightness profile is well fitted by a single Sérsic law along its whole radius range (i.e. it does not show two components). However, the S0 morphological classification assigned to this galaxy by FS90 is in agreement with the B4 coefficient values that point to discy isophotes, and with the red inner disc found in its $(C - T_1)$ colour map and confirmed through unsharp masking. There are no images from VLT or *HST* for this object.

### 5.2 FS90 208

Certainly, FS90 208 is not a cE galaxy either. It is a confirmed Antlia member that follows the same fundamental relations as FS90 165 and the rest of the low surface brightness early-type galaxies, and it is not compact. Besides, it is not close in projection to any bright galaxy and is far from the centre of the cluster. However, it displays a two-component brightness profile and presents important variations in ellipticity and position angle that resemble those shown by M32 (Choi et al. 2002), albeit stronger. Curiously, these variations arise at the same galactocentric radii as those displayed by FS90 110, and behave in a similar way. FS90 have classified this object as an S0 galaxy, which is in agreement with the two components present in its brightness profile, as well as with the B4 coefficient, which indicates that the isophotes are nearly discy. Moreover, a process of unsharp masking reveals what seems to be an inner bar structure, slightly detected with the subtraction of a fixed ELLIPSE model of the galaxy from the MOSAIC image. However, a triaxial object, in which the axial ratios vary with radius, could also display isophote twisting (Binney & Merrifield 1998).

### 5.3 FS90 192

There is no radial velocity available for FS90 192. It displays no perceptible colour gradients and, if it were an Antlia member, it would be as compact as other cE galaxies. Furthermore, its projected distance to NGC 3268 would be smaller than that between NGC 4486B and NGC 4486. Although it does not display two components in its brightness profile, it is worth noting that NGC 4486B in the Virgo cluster also presents a single-component profile and a similar $n$ (i.e. $1/N$) value.

Despite all the interesting features mentioned above, we cannot confirm or rule out that this object is in the background. It does not follow the fundamental relations of early-type Antlia members, as it appears shifted towards higher surface brightnesses, fainter magnitudes or redder colours. M32 would hold a comparable position on the colour–magnitude diagram if it were placed at the Antlia distance. However, FS90 192 does not follow the relation between mean effective surface brightness and luminosity defined by confirmed cEs. Under the hypothesis that it is a background object, FS90 192 would become an isolated elliptical galaxy of moderate

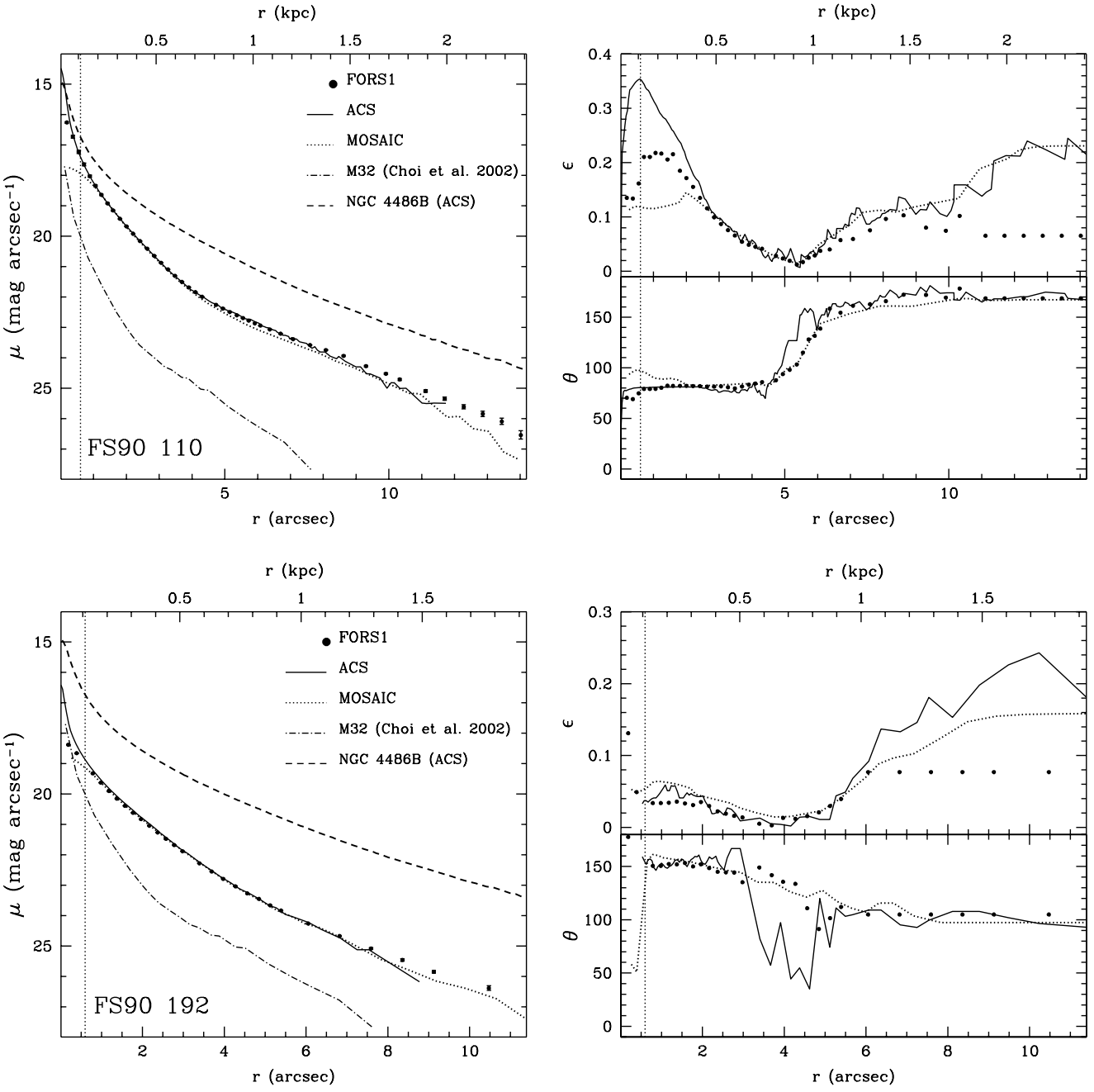


**Figure 8.** Left: $T_1$ brightness profiles of FS90 110 (top) and FS90 192 (bottom), compared with the *V* profile obtained from FORS1, and the *I* profile obtained from ACS. The FORS1 profiles have been shifted by adding 1.1 mag in order to match the $T_1$ profiles, and the ACS profiles by adding 0.4 mag. We have also added the *z* ACS brightness profile of NGC 4486, and that of M32 in the *I* band from Choi et al. (2002), with their equivalent radius rescaled to the Antlia distance. For clarity, the M32 profile has been shifted by adding 2.5 mag. Right: comparison of ellipticity and position angle versus equivalent radius of FS90 110 and FS90 192, obtained from MOSAIC, FORS1 and ACS images (symbols as in the left panel). The vertical dotted lines in all panels show the seeing region of the FORS1 images. The equivalent radius scale displayed at the top of all panels was obtained considering the adopted Antlia distance (1 arcsec $\simeq$ 170 pc).

luminosity (highly unlikely), as we have not found any concentration of galaxies in its neighbourhood.

### 5.4 FS90 110

There is no radial velocity available for FS90 110 and, as stated in Section 3.4, it could be a background galaxy placed at $\sim$120 Mpc. However, it seems to be the most firm candidate for a cE galaxy.

If it were an Antlia member, its projected separation from NGC 3258 would be of the same order as those of M32 from M31 and NGC 5486A from NGC 5486. Moreover, it would be much closer to the dominant galaxy than NGC 4486B to NGC 4486, and its effective radius would be smaller than that of NCG 5846A.

It presents a high central surface brightness in the brightness profile obtained from the ACS image, and its $(C - T_1)$ and $(V - I)$ colour profiles are flat, in agreement with what is found for M32.

**Table 4.** FS90 cE candidates located in the FORS1 images. $\mu_V$ gives the surface brightness of the outermost isophote within which integrated magnitudes and colours are measured. $r_V$ is the equivalent radius ($r = \sqrt{ab}$) of that isophote. $\langle\mu_{\rm eff}\rangle$ is obtained from $r_{\rm eff}$. All these values were obtained from ELLIPSE.

| FS90 ID | $V$ (mag) | $(V-I)$ (mag) | $\mu_V$ (mag arcsec$^{-2}$) | $r_V$ (arcsec) | $\langle\mu_{\rm eff}\rangle_V$ (mag arcsec$^{-2}$) | $r_{{\rm eff}_V}$ (arcsec) |
|---|---|---|---|---|---|---|
| 110 | 16.41 | 1.14 | 27.7 | 12.3 | 18.8 | 1.2 |
| 192 | 18.00 | 1.21 | 27.3 | 8.6 | 21.0 | 1.6 |

Its brightness profile shows two components in the equivalent radius range 2–11.8 arcsec, which seems to be described by $N > 1$ (i.e. $n < 1$) Sérsic indices. It is tempting to suggest that such an $N$ index for the outer component might be linked to a truncation of the profile (Erwin et al. 2008), because of a possible interaction with NGC 3258. However, such a hypothesis should be studied in light of the confirmed membership status of FS90 110. Furthermore, it would be interesting to test whether the outer component of confirmed cE galaxies displaying two components in their brightness profiles could be fitted by a Sérsic law with $N > 1$ (i.e. $n < 1$).

The variations of the ellipticity and position angle versus radius displayed by FS90 110 resemble those found in M32. These changes occur at a galactocentric radius at which the outer component seems to begin to dominate, in agreement with what Graham (2002) found for M32.

FS90 110 is the only FS90 cE candidate that follows the luminosity versus mean effective surface brightness relation defined by bright ellipticals, which corresponds to the Kormendy (1977) scaling relation, towards fainter magnitudes, smaller radius or higher mean effective surface brightness. It also seems to follow the colour–magnitude relation of Antlia members, although it is located at the red border.

The elongation and twisting of FS90 110's outermost isophotes in the direction of NGC 3258 are noticeable. This would be consistent with the extremely low surface brightness structure detected in the MOSAIC images, and confirmed with the FORS1 and ACS frames. Such a 'bridge', which seems to link FS90 110 with its bright partner, would be in agreement with the fact that most confirmed cE galaxies are located in the vicinity of brighter companions. In this sense, it is also worth noting the warped inner structure displayed in the ACS colour map, and confirmed through unsharp masks of FORS1. Similar stellar structures are found in numerical simulations (Bekki et al. 2001; Mayer et al. 2006) as a consequence of galaxy interactions.

### 5.5 Final remarks

A galaxy that is interacting with a more massive partner will feel tidal forces most strongly in its outskirts, while its central region will be less affected (see, for example, Bekki et al. 2001, for a model of the interaction between M32 and M31). As a consequence, it would not be surprising to observe asymmetric and 'egg-shaped' outer isophotes, and/or to detect low surface brightness stellar 'tails', arising from the disruption of the outer regions of the satellite (Mayer et al. 2006). In particular, these faint structures could be observed either as one or two symmetric 'tails', depending on projection effects (see fig. 4 in Mayer et al. 2006). The distorted outermost isophotes of FS90 110 and the extremely faint structure detected in the *HST*, VLT and CTIO images fit well in such a scenario.

The similarities in the ellipticity and position angle variations against radius displayed by FS90 110 and FS90 208, which arise at a similar galactocentric radius of ∼5.5 arcsec (i.e. in their inner regions), are also remarkable. These types of variation have already been detected in M32, although not so strongly. All this evidence leads us to speculate about the possibility that an object similar to FS90 208 might be the progenitor of a cE galaxy. Thus, it is tempting to look for possible links between these two types of object.

We may think that a system with similar characteristics to FS90 208 may lose its outermost regions as a result of interaction with a bright companion, then becoming compact. As a consequence, it could also experience a redistribution of its stellar content, which might produce a warped inner structure, a higher central surface brightness and an attenuation of its ellipticity and position angle variations with radius. Moreover, the bulge-to-disc ratio in such an object could increase after losing its outer parts because of the interaction. With regard to this point, it should be noted that the inner component of FS90 110 seems to be three times brighter than the outer component, while that of FS90 208 is just 1.6 times brighter in relation with the outer component.

As an additional point, we recall that the Antlia cluster seems to be particularly rich in S0 galaxies, and FS90 208 seems to be one of these. If the evolutionary path of cE galaxies include this type of object, S0-rich clusters would arise as favourable environments for the formation of compact galaxies.

Dynamical simulations and the spectroscopically confirmed membership status of FS90 110 and FS90 192 will help to test whether any of the above statements are indeed plausible.

## ACKNOWLEDGMENTS

We would like to thank the referee, Igor Chilingarian, for his useful comments that helped to improve this paper. We are also grateful to S. A. Cellone for valuable discussions and for kindly reading the original manuscript. This research has made use of the NASA/IPAC Extragalactic Database (NED), which is operated by the Jet Propulsion Laboratory, California Institute of Technology, under contract with the National Aeronautics and Space Administration. This work was funded with grants from Consejo Nacional de Investigaciones Científicas y Técnicas de la República Argentina, Agencia Nacional de Promoción Científica Tecnológica and Universidad Nacional de La Plata (Argentina). TR is grateful for support from the Chilean Center for Astrophysics, FONDAP No. 15010003.

## REFERENCES

Alonso M. V., Bernardi M., Da Costa L. N., Wegner G., Willmer C. N. A., Pellegrini P. S., Maia M. A. G., 2003, AJ, 125, 2307
Bassino L. P., Richtler T., Dirsch B., 2008, MNRAS, 386, 1145
Bekki K., Couch W. J., Drinkwater M. J., Gregg M. D., 2001, ApJ, 557, L39
Binggeli B., Sandage A., Tammann G. A., 1985, AJ, 90, 1681
Binney J., Merrifield M., 1998, in Galactic Astronomy, Princeton Series in Astrophysics. Princeton Univ. Press, Princeton, NJ, p. 184
Canterna R., 1976, AJ, 81, 228
Cellone S. A., Buzzoni A., 2001, A&A, 369, 742
Cellone S. A., Buzzoni A., 2005, MNRAS, 356, 41
Chilingarian I., Cayatte V., Chemin L., Durret F., Laganá T. F., Adami C., Slezak E., 2007, A&A, 466, L21
Chilingarian I., Cayatte V., Durret F., Adami C., Balkowski C., Chemin L., Laganá T. F., Prugniel P., 2008, A&A, 486, 85
Choi P. I., Guhathakurta P., Johnston K. V., 2002, AJ, 124, 310
Conselice C. J., Gallagher J. S., Wyse R. F. G., 2002, AJ, 123, 2246
Davidge T. J., 1991, AJ, 102, 896

de Vaucouleurs G., de Vaucouleurs A., Corwin H. G., Buta R. J., Paturel G., Fouque P., 1991, Third Reference Catalogue of Bright Galaxies. Springer-Verlag, New York (RC3)
Dirsch B., Richtler T., Bassino L. P., 2003, A&A, 408, 929
Djorgovski S., Davis M., 1987, ApJ, 313, 59
Drinkwater M. J., Gregg M. D., Holman B. A., Brown M. J. I., 2001, MNRAS, 326, 1076
Erwin P., Pohlen M., Beckman J. E., 2008, AJ, 135, 20
Ferguson H. C., Sandage A., 1990, AJ, 100, 1 (FS90)
Ferrarese L. et al., 2006, ApJS, 164, 334
Forbes D. A., Forte J. C., 2001, MNRAS, 322, 257
Forte J. C., Faifer F. R., Geisler D., 2007, MNRAS, 382, 1947
Fukugita M., Shimasaku K., Ichikawa T., 1995, PASP, 107, 945
Gavazzi G., Donati A., Cucciati O., Sabatini S., Boselli A., Davies J., Zibetti S., 2005, A&A, 430, 411
Geisler D., 1996, AJ, 111, 480
Graham A. W., 2002, ApJ, 568, L13 (erratum ApJ, 572, L121)
Graham A. W., Worley C. C., 2008, MNRAS, 388, 1708
Graham A. W., Jerjen H., Guzmán R., 2003, AJ, 126, 1787
Jedrzejewski R. I., 1987, MNRAS, 226, 747
Jerjen H., Kalnajs A., Binggeli B., 2000, A&A, 358, 845
Kormendy J., 1977, ApJ, 218, 333
Lauer T. R. et al., 1996, ApJ, 471, L79
Lisker T., Glatt K., Westera P., Grebel E. K., 2006a, AJ, 132, 2432
Lisker T., Grebel E. K., Binggeli B., 2006b, AJ, 132, 497
MacArthur L. A., Courteau S., Holtzman J. A., 2003, ApJ, 582, 689
Mahdavi A., Trentham N., Tully R. B., 2005, AJ, 130, 1502
Mateo M. L., 1998, ARA&A, 36, 435
Mayer L., Mastropietro C., Wadsley J., Stadel J., Moore B., 2006, MNRAS, 369, 1021
Mieske S., Infante L., Hilker M., Hertling G., Blakeslee J. P., Benítez N., Ford H., Zekser K., 2005, A&A, 430, L25
Nakazawa K., Makishima K., Fukazawa Y., Tamura T., 2000, PASJ, 52, 623
Nieto J.-L., Prugniel P., 1987, A&A, 186, 30
Pedersen K., Yoshii Y., Sommer-Larsen J., 1997, ApJ, 485, L17
Peletier R. F., 1993, A&A, 271, 51
Rose J. A., Arimoto N., Caldwell N., Schiavon R., Vazdekis A., Yamada Y., 2005, AJ, 129, 712
Sánchez-Blázquez P., Gorgas J., Cardiel N., 2006, A&A, 457, 823
Sandage A., Binggeli B., 1984, AJ, 89, 919
Schlegel D., Finkbeiner D., Davis M., 1998, ApJ, 500, 525
Sérsic J. L., 1968, Atlas de Galaxias Australes. Obs. Astron., Univ. Nac. Córdoba, Córdoba
Sirianni M. et al., 2005, PASP, 117, 1049
Smith Castelli A. V., Bassino L. P., Richtler T., Cellone S. A., Aruta C., Infante L., 2008, MNRAS, 386, 2311 (Paper I)
Tonry J. L., Dressler A., Blakeslee J. P., Ajhar E. A., Fletcher A. B., Luppino G. A., Metzger M. R., Moore C. B., 2001, ApJ, 546, 681
Trujillo I., Aguerri J. A. L., Cepa J., Gutiérrez C. M., 2001a, MNRAS, 321, 269
Trujillo I., Aguerri J. A. L., Cepa J., Gutiérrez C. M., 2001b, MNRAS, 328, 977
Ziegler B. L., Bender R., 1998, A&A, 330, 819

This paper has been typeset from a TEX/LATEX file prepared by the author.